

HF Characterization and Nonlinear Modeling of a Gapped Toroidal Magnetic Structure

Luca Dalessandro, *Student Member, IEEE*, Willem G. Hardus Odendaal, *Senior Member, IEEE*, and Johann W. Kolar, *Senior Member, IEEE*

Abstract—The frequency dependent characteristics of a gapped toroidal structure are extracted empirically over a bandwidth that exceeds 30 MHz. The analysis is complicated due to nonlinear flux distributions, magnetic properties of the core material, leakage inductance, stray capacitances, and eddy currents in the windings. A permeance model of the core is implemented to model the magnetic circuit. The model includes a linear lumped element equivalent circuit to approximate the nonlinear complex permeability of the core, which was measured empirically. Stray capacitance and inductance of the winding are also modeled. A gyrator is used to couple the electric and magnetic models for circuit simulation. The measured and simulated results of open-circuit impedance from the secondary winding and the transimpedance gain (V/A) of the current sensor are compared and discussed.

Index Terms—Gapped toroidal structure, nonlinear flux distributions.

I. INTRODUCTION

THE wide-band characteristics of passive components are becoming increasingly important even for high power applications, for which there has been a steady increase in switching frequencies over recent years. Present microprocessors are more able to cope with high frequencies and enable tighter control bandwidth. The ability to predict conducted electromagnetic interference (EMI) in power electronics circuitry before even constructing a prototype has also become a reality. These are only some of the reasons why high frequency behavior will gain increasing interest for the accurate characterization, modeling, and design of circuit components, such as filters, inductors, capacitors, and sensors, for frequencies typically up to 30 MHz.

Current transformers with high frequency bandwidths are of special interest, since they are widely used in electromagnetic compatibility (EMC) compliance testing to inject disturbances as well as in power electronics circuits with high switching frequencies and wide-band control functions [1]. This manuscript investigates the high frequency behavior of a gapped toroidal magnetic structure which is intended for a current sensor application. In practice, the application includes a Hall-effect element, which is physically positioned in the air-gap as shown

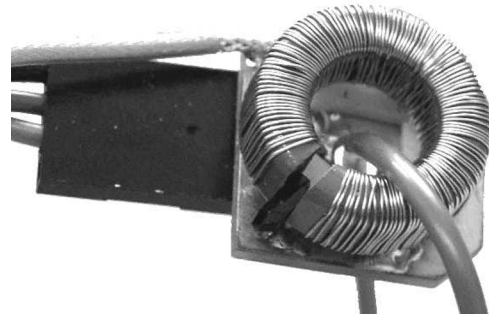


Fig. 1. Prototype of dc-broadband CT showing the wound toroid with a Hall-element positioned in the air gap.

in Fig. 1, for dc and low frequency components of the measured current. The higher frequencies, to which the Hall-sensor is insensitive, are detected magnetically. The magnetic structure, which will be considered herein, thus consists of a toroidal core with an air-gap, a single-turn primary passing through the center window of the core, and a multi-turn secondary winding connected to the detection circuitry via a small load resistor. Even though this is in principle a rather simple structure, its behavior at high frequencies is affected by several factors that can produce highly nonlinear response signals.

First, a large air-gap (necessitated by the physical dimensions of the Hall-element) in a toroidal core produces a large distribution of fringing flux that leaks through the window of the core instead of passing through the air gap. This irregular distribution of flux depends on the winding arrangement. Second, the core characteristics become nonlinear due to the frequency-dependent behavior of the ferrite core. At higher frequencies rotational magnetic losses dominate, and the dielectric properties of the material play an increasing role. Last, the secondary winding itself exhibits enough stray capacitance and stray inductance to affect performance, notwithstanding the internal impedances which give rise to a substantial higher resistance due to eddy current effects. The complexity of its behavior due to the combination of the above effects does not only affect the modeling of the structure, but also its empirical characterization. In [2], the difficulties and tradeoffs associated with wide-band characterization of a current probe by means of frequency domain, S -parameter testing and time domain testing were discussed. In this study, a lumped element model is extracted using impedance measurements and the dominating design parameters that dictate broadband performance are also identified. A permeance model of the core is implemented to model the magnetic circuit and stray capacitance and inductance of the winding are also included. The model includes a linear lumped element equivalent circuit to approximate the nonlinear complex permeability of

Manuscript received July 7, 2005; revised January 4, 2006. This work was supported in part by the PES Laboratory, ETH Zurich, Switzerland. Recommended by Associate Editor F. Blaabjerg.

L. Dalessandro and J. W. Kolar are with the Power Electronic Systems Laboratory, Swiss Federal Institute of Technology (ETH) Zurich, Zurich CH-8092, Switzerland (e-mail: dalessandro@lem.ee.ethz.ch; kolar@lem.ee.ethz.ch).

W. G. Hardus Odendaal is with the NSF Engineering Research Center for Power Electronics Systems (CPES), Virginia Polytechnic Institute and State University, Blacksburg, VA 24060 USA (e-mail: hardus@ieee.org).

Digital Object Identifier 10.1109/TPEL.2006.880357

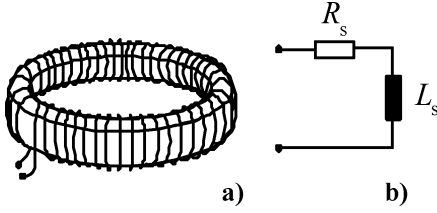


Fig. 2. (a) Fully wound thin toroid for the measurement of complex permeability and (b) its equivalent circuit.

the core, which was measured experimentally. A set of gyrators is used to couple the electric and magnetic models for circuit simulation.

II. CORE MATERIAL CHARACTERIZATION

A. Measurement of Complex Permeability

Complete material information over a broad frequency bandwidth is not always available. Therefore, the measurement of the fundamental ferrite parameters, i.e., permeability, permittivity, and conductivity must often be performed by the magnetic designers themselves. For this aim, specific material samples must be used. The complex relative permeability $\mu_r = \mu' - j\mu''$ can be extracted by measuring the reactance of a thin toroidal core (see Fig. 2). Since the dimensional effects influence this kind of measurement, the core cross section should be sufficiently small [3]–[5]. Moreover, the windings on the sample core should ideally wrap fully around the circumference of the toroid. This uniform winding reduces the amount of flux that leaves the core and forces a more uniform flux density distribution in the core. The impedance Z of an N -turn inductor L can be represented at any given frequency $\omega/2\pi$ by the series combination of a resistance R_s and a reactance $j\omega L_s$

$$\begin{aligned} j\omega L &= j\omega\mu_o\mu_r \left(\frac{N^2 A_e}{l_e} \right) \\ &= j\omega\mu_o(\mu' - j\mu'') \left(\frac{N^2 A_e}{l_e} \right) \\ &= j\omega \left(\frac{\mu_o\mu' N^2 A_e}{l_e} \right) + 2\pi f \left(\frac{\mu_o\mu'' N^2 A_e}{l_e} \right) \\ &= j\omega L_s + R_s \end{aligned} \quad (1)$$

where A_e is the effective core cross section and l_e is the mean flux path length. The values of equivalent series circuit parameters R_s and L_s can be measured directly using an impedance analyzer. The real and imaginary parts of the complex relative permeability are then obtained from

$$\mu'(f) = L_s(f) \left(\frac{l_e}{\mu_o N^2 A_e} \right) \quad (2)$$

$$\mu''(f) = R_s(f) \left(\frac{l_e}{2\pi f \mu_o N^2 A_e} \right). \quad (3)$$

An R4 toroidal core of N30 ferrite, having dimensions $d_{\text{ext}} = 4$ mm, $d_{\text{int}} = 2.4$ mm, $h = 1.6$ mm, was used for the measurement. This thin toroid was fully wound with $N = 22$ turns. The impedance was measured with an Agilent A294A Precision Impedance Analyzer with an oscillation level of 0.5 mA

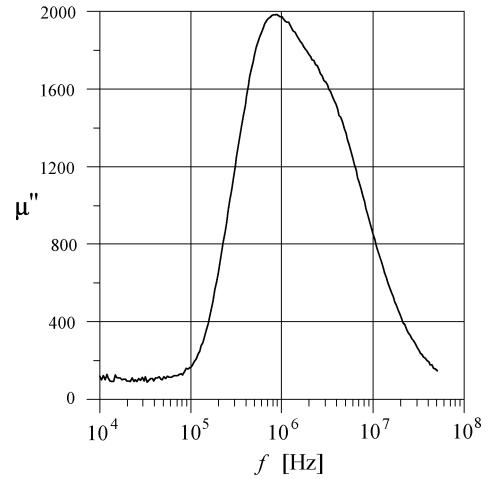
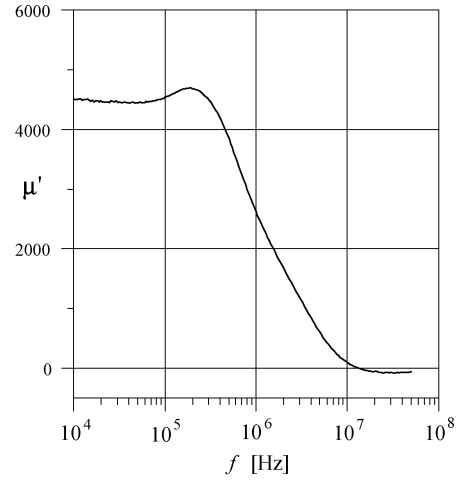


Fig. 3. Frequency plot of the real and imaginary parts μ' and μ'' , respectively, of the complex relative permeability for N30 ferrite at 25 °C.

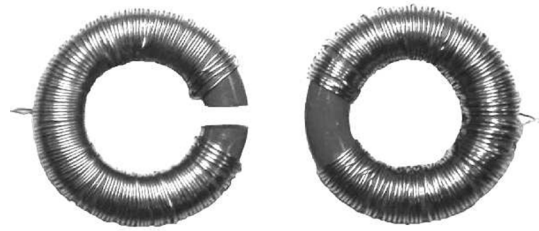


Fig. 4. Prototypes of the broadband dc-CT. Ungapped toroids were used for empirical characterization.

The results shown in Fig. 3 are in good agreement with similar measurements obtained for larger cores [6].

B. Prototype Construction

The magnetic cores selected for the measurements were R16 toroidal cores of N30 ferrite. Two designs were prototyped for testing; one having an air gap of 1.6 mm and another without an air gap as shown in Fig. 4.

C. Winding Arrangement

High immunity against external fields is important especially for current measurement applications. The winding arrangement must therefore be chosen carefully so that any external

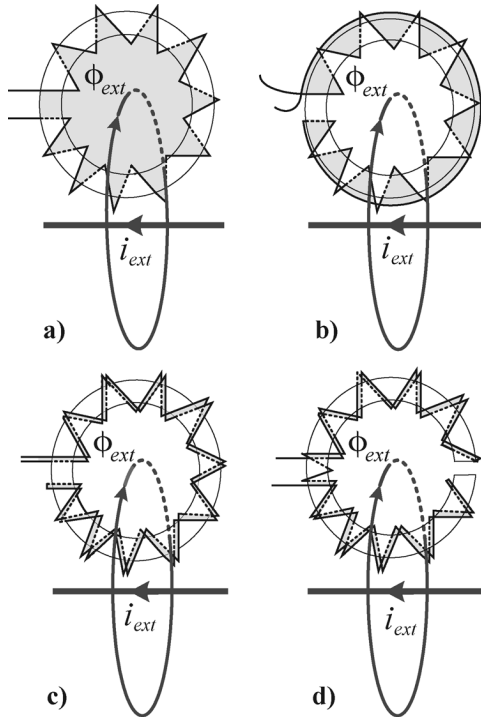


Fig. 5. Effect of an external magnetic field for different winding arrangements on toroidal magnetic cores. The cross-sectional area of flux linkage in (a) becomes smaller if a conductor is returned to the starting position as shown in (b). This loop area reduces further if the return conductor is wound as shown in (c). For a gapped toroid, such as in (d), the arrangement must be repeated twice.

magnetic fields will not influence the sensor accuracy [7]. If a traditional winding is realized, as in Fig. 5(a), then the area linked with the external magnetic field is about equal to the internal circumference of the toroid. If one of the two terminals is returned back along the outer circumference of the toroid, then the loop area is reduced as in Fig. 5(b). This solution is usually used for realizing Rogowski coils [8]–[10]. If the return conductor is also wound as in Fig. 5(c), then the loop area is further reduced. For a gapped toroid, this latter winding strategy can be realized as shown in Fig. 5(d).

The secondaries of the prototypes consisted of 120 turns of 0.2-mm magnet wire.

III. MAGNETIC MODELING USING PERMEANCES

The capacitance–permeance model [11]–[13] was chosen to model the rotational magnetization losses of the magnetic core. The model allows electrical simulation of a nonlinear magnetic structure, through an analogous transformation of field quantities and the implementation of a gyrator. In an electrical analogous model, the relationship between capacitance and charge from

$$\frac{dq}{dt} = C \frac{dv}{dt} \quad (4)$$

can be written as

$$C = \frac{dq}{dv}. \quad (5)$$

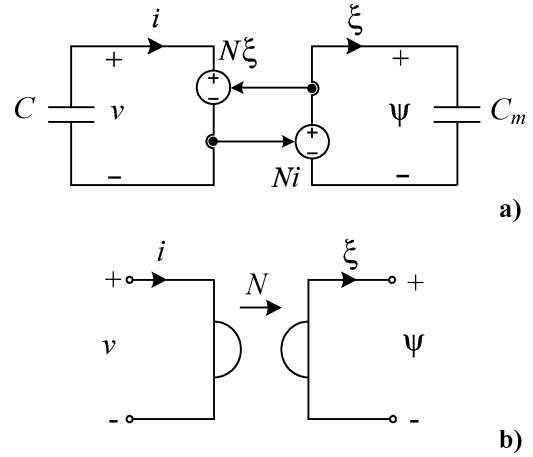


Fig. 6. (a) Equivalent circuit that implements the coupling between electrical and magnetic domains using the capacitance–permeance analogy. (b) Symbol of the Tellegen gyrator.

A permeances model is then constructed by defining the permeance C_m in henries per turn square as

$$C_m = \frac{d\varphi}{d\psi}. \quad (6)$$

The magnetomotive force (MMF) per turn ψ in ampères is used analogous to the voltage in an electrical equivalent, whereas the induced voltage per turn ξ in wb/s is used analogous to the current

$$\xi = \frac{d\varphi}{dt}. \quad (7)$$

This model is easily verified by expanding (6)

$$C_m = \frac{\partial \mathbf{B} \cdot \mathbf{S}}{\partial \mathbf{H} \cdot \mathbf{1}} = \frac{\mu \partial \mathbf{B} \cdot \mathbf{S}}{\partial \mathbf{B} \cdot \mathbf{1}}, \quad (8)$$

where $\varphi = \mathbf{B} \cdot \mathbf{S}$, $\psi = \mathbf{H} \cdot \mathbf{1}$, and $\mathbf{B} = \mu \mathbf{H}$. \mathbf{B} is the induction, \mathbf{H} is the magnetic field, and \mathbf{S} and $\mathbf{1}$ are the oriented cross-sectional area and the flux pathlength, respectively. If normal uniform field distributions are assumed in the media considered, then the permeance is the reciprocal of the reluctance analogy

$$C_m = \frac{\mu S}{l} = \mathfrak{R}^{-1}.$$

A gyrator (see Fig. 6) is implemented to link the equivalent magnetic circuit to the electrical domain

$$\begin{aligned} \psi &= Ni \\ v &= N\xi. \end{aligned} \quad (9)$$

In a circuit simulator the magnetic circuit can thus be constructed using capacitor elements to represent all of the permeances. In the magnetic domain, the flux path may be broken into series capacitor elements representing permeances, whereas the flux cross section may be broken into parallel capacitor elements representing permeances. For instance, a core with an air gap is modeled as a capacitor for the core permeance in series with a

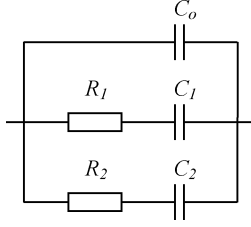


Fig. 7. Equivalent magnetic circuit for the complex permeability using linear lumped electrical elements.

TABLE I
PARAMETERS FOR COMPLEX PERMEABILITY OF N30 FERRITE

μ_r		permeance	
name	value	name	value
χ_1	2.621×10^3	C_o	671.5 pF
χ_2	1.599×10^3	C_1	1.76 μ F
τ_1	4.385×10^{-11}	C_2	1.074 F
τ_2	6.943×10^{-11}	R_1	65 m Ω
		R_2	103 m Ω

capacitor representing the permeance of the air gap. The connection to the electrical circuit can then be represented by the Tellegen gyrator according to (9), comprising a controlled voltage source producing ψ (in series with the two capacitors), and another controlled voltage source producing the electrical voltage.

A. Modeling the Nonlinear Magnetic Core

If the frequency dependency of the ferrite core permeability is to be included in the model, then a simple curve fit may be implemented to approximate the complex permeability as a function of frequency. For frequencies up to 200 MHz, the permeability is then approximated by assuming that

$$\mu_r(j\omega) = 1 + \frac{1}{1 + j\omega\chi_1\tau_1} + \frac{1}{1 + j\omega\chi_2\tau_2}. \quad (10)$$

Formula (10) is a description of the complex permeability through relaxation effects. χ_1 and χ_2 represent the low frequency susceptibilities of the domain wall movement and rotational magnetic losses respectively. The time constants τ_1 and τ_2 are material properties. For a toroid having a cross section S and a magnetic path length l , the nonlinear permeance of the core can be represented by a circuit comprising linear elements as shown in Fig. 7. For N30 ferrite, Table I lists the curve-fitted values that were obtained empirically and subsequently used in the simulations.

The relationship between this model and the parameters for complex permeability is treated in the Appendix.

IV. EMPIRICAL CHARACTERIZATION OF THE PROTOTYPE CURRENT TRANSFORMER STRUCTURE

A. Open Circuit Impedance

The device under test is in essence a current transformer (CT) with a single conductor in the primary. A model for

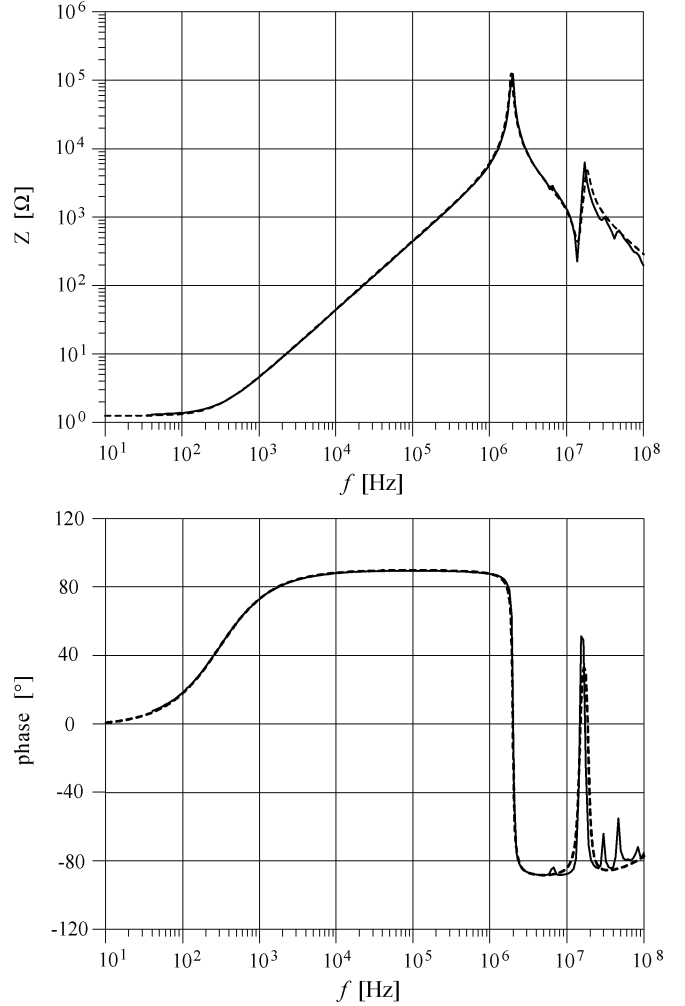


Fig. 8. Plots of measured (solid line) and simulated (dashed line) output impedance.

the secondary winding was extracted by measuring its output impedance with an open-circuited primary conductor still present. Rigorous methods for modeling winding impedances are given in [14] and [15]. The measured and simulated results are plotted in Fig. 8 and the equivalent circuit for the simulation is depicted in Fig. 9. The lumped equivalent circuit model for the winding approximates the effects of winding stray capacitances, the winding leakage impedance and the high frequency ac resistance for the frequency range of interest. It can be extended to include higher order resonances that occur for frequencies beyond 30 MHz.

B. Transimpedance Gain

The primary was fed by a signal of constant amplitude over the frequency range 250 kHz to 30 MHz using a signal generator and a power amplifier as shown in Fig. 10, and a list of the equipment is given in Table II. The primary of the CT consists of a custom designed coaxial construction that provides a constant resistance of 50 Ω up to 30 MHz. It allows better stability over this frequency range and also matches the output impedance of the power amplifier. At each frequency, the primary (input) current amplitude I_1 and the secondary (output) voltage amplitude U_L across the load resistor R_L are measured, along with the time

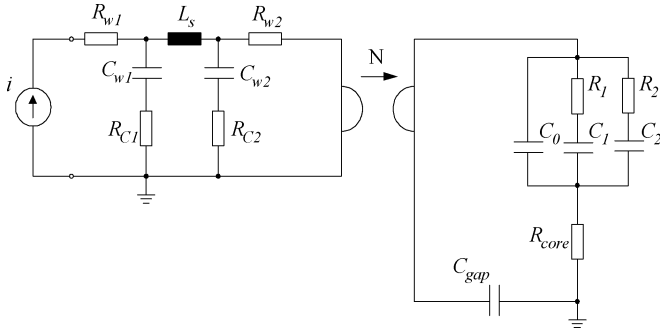


Fig. 9. Equivalent circuit with core permeances model and extracted winding impedances for simulating the output impedance measurement.

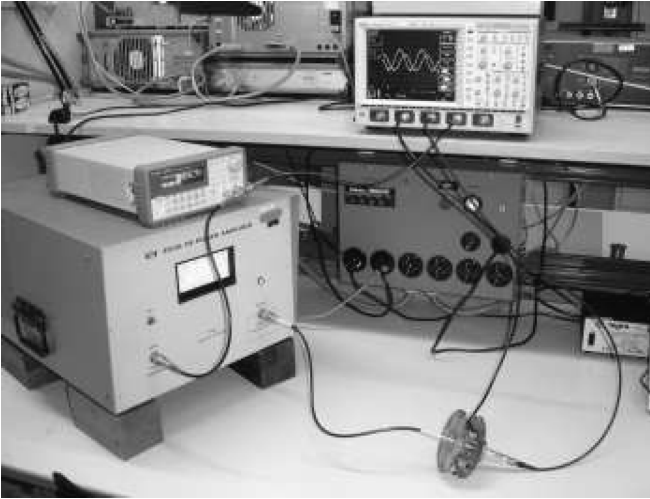


Fig. 10. Photograph of the experimental setup.

TABLE II
LIST OF EQUIPMENT

Signal Generator	Agilent 33250A 80 MHz function/arbitrary waveform generator
Power Amplifier	ENI 3200L RF Power Amplifier gain 55 dB, 250 kHz-150 MHz
50Ω Coaxial Primary	custom design 50 MHz bandwidth
50mΩ Shunt	T&M Research Products Model A-1-05, $E_{max} = 20$ J
Oscilloscope	LeCroy Waverunner LT584L 1 GHz
Voltage Probe	LeCroy PP006A 500 MHz

delay between the two signals i_1 and u_L , that provides the difference $\Delta\varphi$ between the phases of the measured signals. The ratio between output voltage and input current provides the transfer function (TF) as a transimpedance gain U_L/I_1 , while the phase of the TF is given by $\Delta\varphi$.

The equivalent circuit of the current transformer for the transimpedance gain simulation is shown in Fig. 12. It includes the core permeances model for the nonlinear core, the equivalent

TABLE III
LOSS BREAKDOWN AT 100 kHz

Part of Circuit	10 A in Primary mW
Source Impedance	71
R_{core}	6.3
Core Non-Linear Network	0.7
Load	63
Winding	1.6

winding impedance, and the two Tellegen gyrators for the secondary winding and the single-turn primary winding.

One of the advantages of the equivalent permeance core model is the ability to compute core losses directly by measuring the power dissipation of the resistors in the magnetic circuit. These losses are tabulated for a 10 A excitation of the primary in Table III.

V. DISCUSSION OF RESULTS

Each circuitual parameter used to model the gapped toroid has a specific physical meaning and influences the frequency behavior of the overall device to some degree according to the frequency of the exciting signal. In particular, the slope of the impedance curve in Fig. 8 depends mainly on the value of the air gap permeance C_{gap} , since most of the magnetic field concentrates in the air gap. The first peak is provided by the parallel resonance between the magnetizing inductance and the winding self-capacitance, the second peak is given by the series resonance between winding leakage inductance L_s and self-capacitance and the third peak by the parallel resonance between L_s and winding self-capacitance. The damping associated with the second and third resonance peaks in the impedance plot, as well as the damping associated with the resonant peak in the transimpedance gain curve (see Fig. 11), are modeled by the two large resistors R_{C1} and R_{C2} . In fact, the core shunt capacitances C_{w1} and C_{w2} cannot simply be grounded since a ferrite material is a poor conductor and the resistors account for the high resistivity of the ferrite.

When the transimpedance gain is calculated (see Fig. 12), then the equivalent circuit remains the same except for the introduction of another gyrator that accounts for the primary and the secondary, which is then closed across a load resistor R_L . A small capacitor between the Tellegen gyrators takes into account leakage flux in the core window that reduces the coupling between the primary conductor and the secondary winding. It is well known that the expression of the transimpedance gain of a transformer for low frequency, i.e., neglecting all HF effects and stray capacitance is

$$\frac{U_L}{I_1} = R_L \left(\frac{sM}{R_L + sL} \right) \quad (11)$$

where L is the self-inductance of the secondary and M is the mutual inductance between primary and secondary [16]. If there is good magnetic coupling between primary and secondary, which is typical for a toroid, then M/L equals the ratio

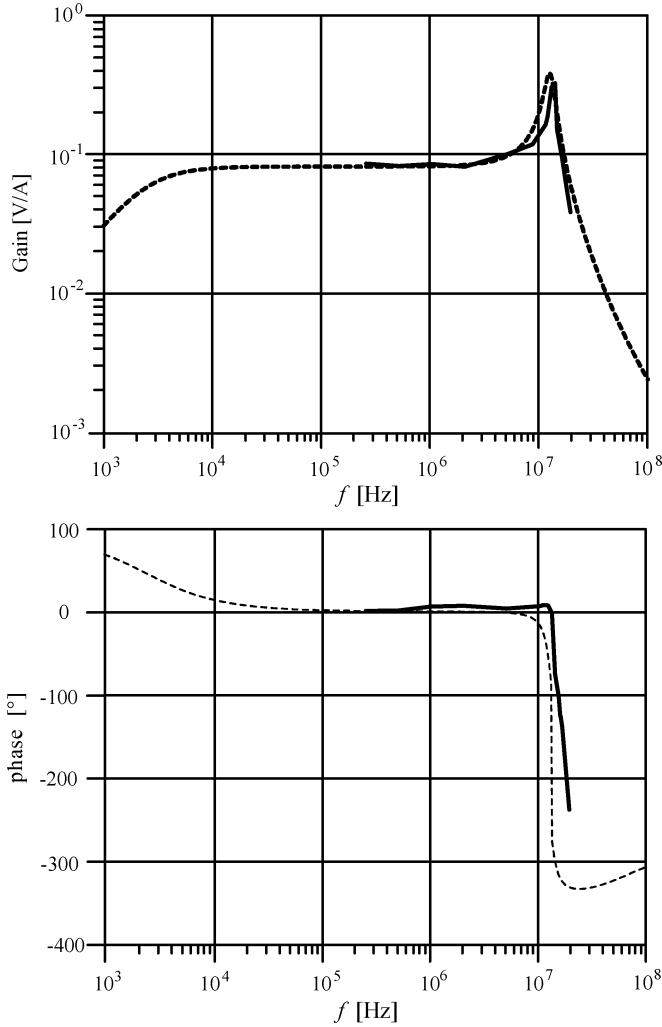


Fig. 11. Measured (solid line) and simulated (dashed line) results of the transimpedance gain of the current transformer.

of primary to secondary turns. Accordingly the low corner frequency and the transimpedance gain are defined as

$$f_L = \frac{R_L}{2\pi L} \quad (12)$$

and

$$\left| \frac{U_L}{I_1} \right| = \frac{R_L}{N}. \quad (13)$$

For this case study these values correspond to $f_L = 2.27$ kHz and $|U_L/I_1| = 83$ m Ω , where $L = 700$ μ H, $R_L = 10$ Ω and $N = 120$ turns. These theoretical values have been verified by the proposed transfer function model (see Fig. 11). If the coupling is not ideal, then the self inductance of the secondary L and the mutual inductance M are not proportional to one another. Therefore, the presence of a small capacitance, C_L between the Tellegen gyrators accounts for the nonideal coupling. Accordingly, the transimpedance gain will be lower and provided by

$$\left| \frac{U_L}{I_1} \right| = R_L \left(\frac{M}{L} \right). \quad (14)$$

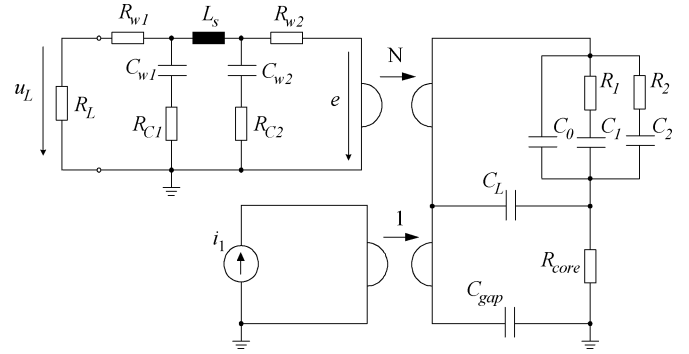


Fig. 12. Equivalent circuit for the current transformer.

Since the leakage inductance L_s is proportional to N^2 and the winding self capacitance C is proportional to N , reducing the number of turns N should extend the frequency band. The drawback of this solution is that the self inductance L will also decrease, thus increasing the lower corner frequency.

The value of the load resistor R_L plays a crucial role in current transformers. First, both the lower corner frequency and the transimpedance gain depend on R_L . If R_L is increased, then a lower amplitude current will flow in the secondary, since the impressed electromotive force (e.m.f.) sMI_1 remains the same. Therefore, the MMF due to the secondary current will compensate just part of the magnetic field associated with the primary current. The magnetic field density and flux line distribution for the inductor are shown in Fig. 13. The compensation of the primary magnetic field by the one in the secondary is evident by examining Fig. 14, where the device operates in the flat part (100 kHz) of its frequency response. For large values of the load resistor or even for open secondary, the primary MMF is not compensated. The flux in the core is basically given by the primary MMF and the device behaves just like an inductor. The magnetizing inductance assumes therefore a larger value and the frequency plots in Figs. 15 and 16 show a prominent first parallel resonance due to the large magnetizing inductance. If R_L is small, then more current will flow in the secondary. Ideally, its amplitude should be equal to the primary current scaled by the turns ratio. In this case, the magnetizing inductance is very small due to flux cancellation so that the resultant flux within the transformer core is negligible. Consequently, for small values of R_L , the magnetizing inductance will have no major influence on the frequency behavior, as is clearly evident from the curves in Figs. 15 and 16.

Fig. 15 depicts the voltage e (see Fig. 12) impressed across the secondary winding for a sinusoidal excitation of 1 A. The voltage e is equal to the flux derivative, which is equivalent to the current flowing in the magnetic loop. In other words, this curve represents the impedance of the secondary winding rescaled by the turn ratio, since it is the primary which is being fed. In particular, the impedance plot in Fig. 8 corresponds to one of the curves in Fig. 15, which was obtained for the largest value of the load resistor. Moreover, the influence of the magnetizing inductance or of the resulting magnetic flux on the shape of the impedance frequency plot is directly apparent from the plots. The results of a similar procedure for the transimpedance gain are depicted in Fig. 16.

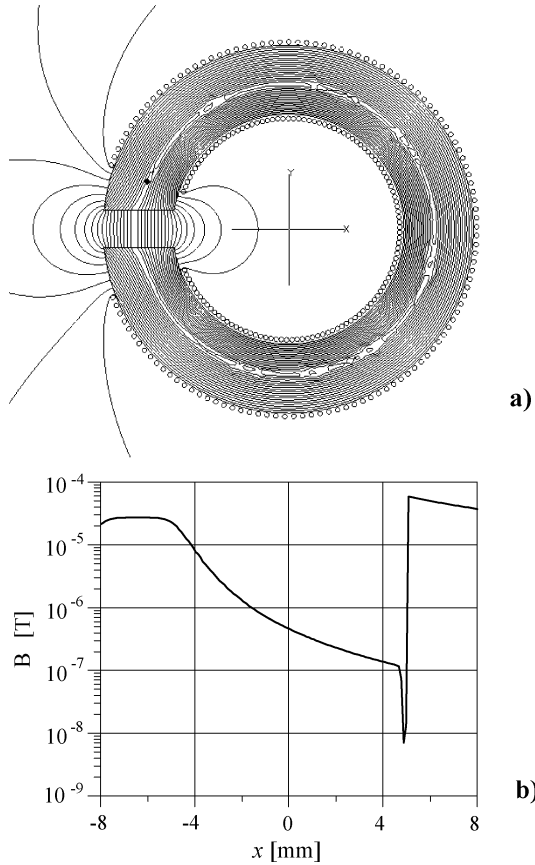


Fig. 13. (a) Magnetic flux distribution for the inductor excited by a MMF of 10 A at 100 kHz. (b) Magnetic flux density B along the x -axis.

VI. CONCLUSION

This investigation of a gapped toroidal magnetic structure for a current sensor dealt with its design, empirical characterization, parameter extraction and modeling over a wide frequency bandwidth up to 30 MHz. In the current sensing application, the Hall-effect sensor provides the low-frequency signal, whereas current transformer action is utilized for the high frequencies. A winding arrangement was presented which desensitizes the probe to the effects of external magnetic fields. The complex permeability of the magnetic core material was measured and the nonlinear behavior of the magnetic core was then modeled by using a permeance model, which also accounts for the core losses. The output impedance was measured and all of the parameters associated with winding stray capacitances, leakage impedance and high frequency winding resistance were extracted for a lumped linear element equivalent circuit that could be linked to the magnetic permeances model via two Tellegen gyrators. The results from these open circuit measurements were compared to simulated results and good agreement was shown. A good agreement was also obtained between the measured transimpedance gain of the current transformer and simulated results thereof using the same models for core permeances and winding impedances. The influence of the load resistance in the secondary circuit on the transimpedance gain was also investigated empirically and numerically.

The upper bandwidth limit of the probe is mostly dependent on the winding impedances, in particular the stray winding capacitances [17], and this was also verified in simulations. The

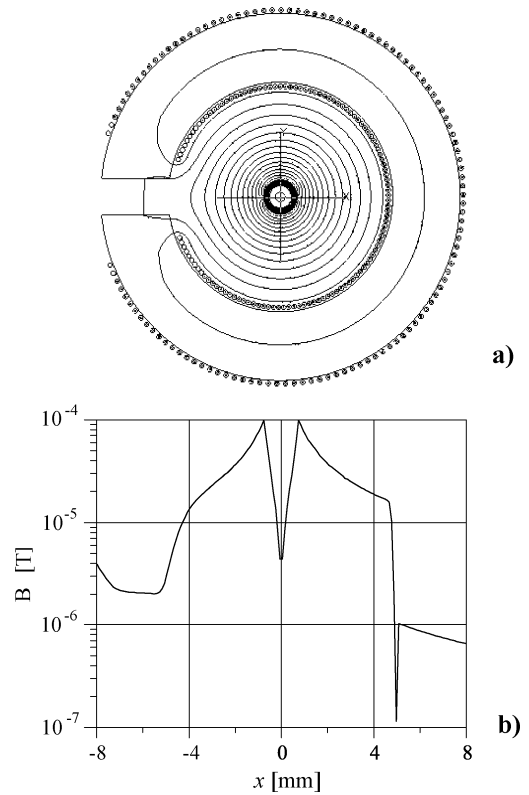


Fig. 14. (a) Magnetic flux distribution for the current transformer excited by a primary current of 10 A at 100 kHz. (b) Magnetic flux density B along the x -axis.

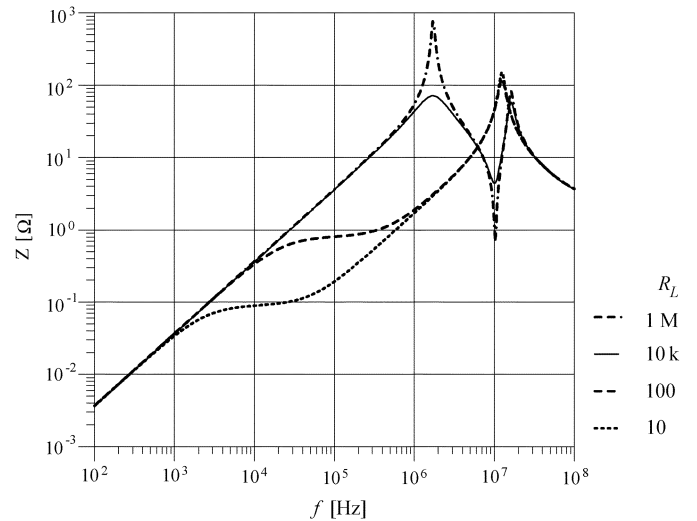


Fig. 15. Frequency behavior as a function of the value of the load resistor R_L of the secondary winding voltage or flux derivative or current in the magnetic circuit over a sinusoidal excitation of 1 A. In particular, the curve for $R_L = 1$ M Ω provides the measured open loop impedance, just rescaled by the turn ratio. The curves were derived by using the equivalent circuit of the current transformer.

permeance model allows access to the flux rate and the MMF in parts of the toroidal core, which provided further valuable information about the magnetic behavior of the magnetic structure. Since a resistance element in the permeance model represents magnetic losses (unlike the conventional magnetic reluctance

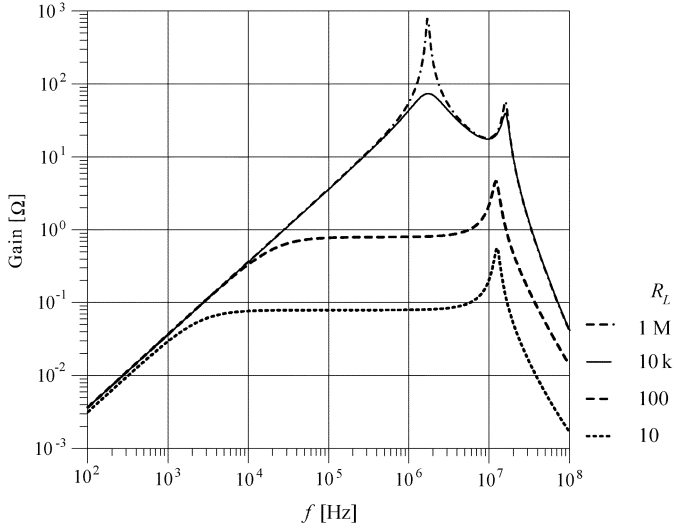


Fig. 16. Transimpedance gain of the current transformer as a function of the value of the load resistor R_L . In particular, the curve for $R_L = 10 \Omega$ corresponds to the case study. The curves are derived by using the equivalent circuit of the current transformer.

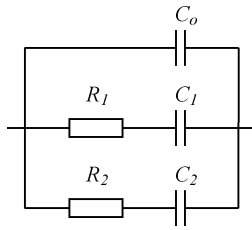


Fig. 17. Equivalent magnetic circuit for the complex permeability using linear lumped electrical elements.

model where resistance represents energy storage), core losses could also be extracted using this method.

The modeling procedure for a gapped toroidal current sensor that is presented herein demonstrates high accuracy for both the winding impedance and the trans-impedance gain. From a practical standpoint, accurate measurement of the transfer function of a current transformer requires much more effort than measuring only its winding impedance, and the characterization of a two port device is generally more complicated than for a one port device. Since the winding impedance measurement and the characterization of the ferrite material allows extraction of all the parameters of the equivalent circuit of the current sensor electrically and magnetically, information about the transfer function of the component can be derived without having to perform any further two port measurements.

APPENDIX

Fig. 17 depicts the equivalent lumped element circuit for representing the frequency-dependent complex permeability of the core, and is repeated here for convenience.

The complex permeability is assumed to obey the function

$$\mu_r(j\omega) = 1 + \frac{1}{1 + j\omega\chi_1\tau_1} + \frac{1}{1 + j\omega\chi_2\tau_2}. \quad (15)$$

The admittance of this circuit in the frequency domain is

$$Y(j\omega) = j\omega \frac{\mu_0 \mu_r(j\omega) A}{l} = j\omega C_o \mu_r(j\omega) = Y_o(j\omega) \mu_r(j\omega) \quad (16)$$

where

$$C_o = \frac{\mu_0 A}{l}. \quad (17)$$

Since C_o can be calculated directly from the geometry, the other four parameters are more easily obtained by subtracting

$$\begin{aligned} \frac{Y(j\omega) - Y_o(j\omega)}{Y_o(j\omega)} &= \frac{Y(j\omega) - j\omega C_o}{j\omega C_o} = \mu_r(j\omega) - 1 \\ &= \left(\frac{C_1/C_o}{1 + j\omega \left(\frac{C_1}{C_o}\right) \left(\frac{R_1}{C_o}\right)} + \frac{C_2/C_o}{1 + j\omega \left(\frac{C_2}{C_o}\right) \left(\frac{R_2}{C_o}\right)} \right). \end{aligned} \quad (18)$$

By inspection, all of the equivalent circuit element values are then identified as follows:

$$\begin{aligned} C_1 &= \chi_1 C_o \\ C_2 &= \chi_2 C_o \\ \tau_1 &= \chi_1 R_1 \\ \tau_2 &= \chi_2 R_2. \end{aligned}$$

The values of χ_1 , χ_2 , τ_1 , and τ_2 can also be obtained by a simple method involving graphical inspection of measured data of the complex permeability. Equation (10) can be simplified as

$$\begin{aligned} \mu_r(j\omega) - 1 &= \frac{1}{1 + j\omega\chi_1\tau_1} + \frac{1}{1 + j\omega\chi_2\tau_2} \\ &= \frac{\chi_1 + \chi_2 + j\omega\chi_1\chi_2(\tau_1 + \tau_2)}{(1 + j\omega\chi_1\tau_1)(1 + j\omega\chi_2\tau_2)} \\ &= A_o \frac{1 + j\omega/\omega_{12}}{(1 + j\omega/\omega_1)(1 + j\omega/\omega_2)} \end{aligned} \quad (19)$$

where

$$\begin{aligned} A_o &= \chi_1 + \chi_2 \\ \omega_1 &= (\chi_1\tau_1)^{-1} \\ \omega_2 &= (\chi_2\tau_2)^{-1} \\ \omega_{12} &= \frac{\chi_1 + \chi_2}{\chi_1\chi_2(\tau_1 + \tau_2)} \\ &= \frac{A_o}{\frac{\chi_2}{\omega_1} + \frac{\chi_1}{\omega_2}}. \end{aligned} \quad (20)$$

The approximate values of ω_1 , ω_2 , and ω_{12} can be determined graphically by identifying asymptotes in a bode plot of the measured $\mu_r - 1$.

The plot of the complex relative permeability of N30 ferrite indicates that it is fair to assume that $\omega_1 < \omega_{12} < \omega_2$. The frequency $(2\pi\tau_2)^{-1}$ is Snoek's limit, which is typically in the order

of several gigahertz for video head ferrites, whereas $(2\pi\tau_1)^{-1}$ lies somewhere between 0.1 and 3 GHz.

ACKNOWLEDGMENT

The authors would like to thank the Staff of SEW-Eurodrive GmbH & Company, for their support, and Dr. N. Karrer and P. G. Blanken, for their helpful input and suggestions.

REFERENCES

- [1] G. Laimer and J. W. Kolar, "Wide-bandwidth low-complexity isolated current sensor to be employed in a 10 kW/500 kHz three-phase unity power factor PWM rectifier system," in *Proc. Power Electron. Spec. Conf.*, 2002, pp. 1065–1070.
- [2] C. Graziano, R. De Leo, V. M. Primiani, S. Pennesi, and P. Russo, "Wide-band characterization of current probes," *IEEE Trans. Electro-magn. Compat.*, vol. 45, no. 4, pp. 616–625, Nov. 2003.
- [3] E. C. Snelling, *Soft Ferrites Properties and Applications*, 2nd ed. London, U.K.: Butterworth, 1988.
- [4] G. R. Skutt, "High Frequency Dimensional Effects in Ferrite-Core Magnetic Devices," Ph.D. dissertation, Virginia Polytechnic Inst. State Univ., Blacksburg, Oct. 1996.
- [5] F. G. Brockman, P. H. Dowling, and W. G. Steneck, "Dimensional effects resulting from a high dielectric constant found in a ferromagnetic ferrite," *Phys. Rev.*, vol. 77, no. 1, pp. 85–93, Nov. 1950.
- [6] EPCOS Ferrites, "Datasheets and Specifications," [Online]. Available: <http://www.epcos.com>, 2004
- [7] R. Prieto, V. Bataller, J. A. Cobos, and J. Uceda, "Influence of the winding strategy in toroidal transformers," in *Proc. Ind. Electron. Soc. Conf.*, Aug./Sep. 1998, vol. 1, pp. 359–364.
- [8] P. N. Murgatroyd, A. K. Y. Chu, G. K. Richardson, D. West, G. A. Yearley, and A. J. Spencer, "Making Rogowski coils," *Meas. Sci. Technol. (2) (Design Note)*, pp. 1218–1219, 1991.
- [9] R. L. Stoll, "Method of measuring alternating currents without disturbing the conducting circuit," *Proc. Inst. Elect. Eng.*, vol. 122, no. 10, pp. 1166–1167, Oct. 1975.
- [10] D. G. Pellinen and P. W. Spence, "A nanosecond risetime megampere current monitor," *Rev. Sci. Instrum.*, vol. 42, no. 11, pp. 1699–1701, Sep. 1971.
- [11] R. W. Buntentbach, "Analogies between magnetic and electrical circuits," *Electron. Prod.*, pp. 108–113, Oct. 1969.
- [12] P. G. Blanken and J. J. L. M. Van Vlerken, "Modeling of electromagnetic systems," *IEEE Tran. Magn.*, vol. 27, no. 6, pp. 4509–4515, Nov. 1991.
- [13] J. J. L. M. Van Vlerken and P. G. Blanken, "Lumped modeling of rotary transformers, heads and electronics for helical scan," *IEEE Tran. Magn.*, vol. 31, no. 2, pp. 1050–1055, Mar. 1995.
- [14] B. Cogitore, J. P. Keradec, and J. Barbaroux, "The two-winding transformer: an experimental method to obtain a wide frequency range equivalent circuit," *IEEE Trans. Instrum. Meas.*, vol. 43, no. 2, pp. 364–371, Apr. 1994.
- [15] A. Schellmanns, P. Fouassier, J. P. Keradec, and J. L. Schanen, "Equivalent circuits for transformers based on one-dimensional propagation: accounting for multilayer structure of windings and ferrite losses," *IEEE Tran. Magn.*, vol. 36, no. 5, pp. 3778–3784, Sep. 2000.
- [16] MIT Staff, *Magnetic Circuits and Transformers* New York: Wiley, 1943.
- [17] P. Wallmeier, P. Ide, J. Kunze, and B. Margaritis, "Effects in magnetic components for switched mode applications in the MHz range," in *Proc. Appl. Power Electron. Conf. Expo*, 2004, vol. 2, pp. 964–970.



Luca Dalessandro (S'02) received the M.Sc. degree (with first class honors) in electrical engineering from the Politecnico di Bari, Bari, Italy, in 2001, and is currently pursuing the Ph.D. degree at the Power Electronic Systems Laboratory (PES), Swiss Federal Institute of Technology (ETH), Zurich.

From 2001 to 2002, he was a Researcher at the Max-Planck-Institute for Mathematics in the Sciences (MPI-MIS), Leipzig, Germany. His research interests include ac-to-dc power conversion, electromagnetics, high performance current sensors, EMC, electromechanical systems modeling and control, and piezoelectricity.

Mr. Dalessandro is a Registered Professional Engineer in Italy.



Willem G. Hardus Odendaal (M'98–SM'04) was born in South Africa in 1969. He received the B.Eng., M.Eng., and D.Eng. degrees in electrical and electronics engineering from Rand Afrikaans University, Johannesburg, South Africa, in 1992, 1995, and 1997, respectively.

He spent one year in a postdoctoral position under two fellowships at the Virginia Power Electronics Center, Virginia Polytechnic Institute and State University (Virginia Tech), Blacksburg, before joining Philips Research North America in New York as

a Senior Member of Research Staff. Since Fall 2001, he has been Assistant Professor in the Bradley Department of Electrical and Computer Engineering, Virginia Tech, as well as a faculty member of the NSF Engineering Research Center for Power Electronics Systems (CPES). His research interests include electromagnetic and thermodynamic energy processing and packaging of power electronic circuits.

Dr. Odendaal is a Member-at-Large of the ADCOM, the IEEE Power Electronics Society and Chairman of the Power Electronics Devices and Components Committee, the IEEE Industry Applications Society.



Johann W. Kolar (M'89–SM'04) received the Ph.D. degree (with highest honors) in industrial electronics from the University of Technology Vienna, Vienna, Austria, in 1984.

From 1984 to 2001, he was with the University of Technology in Vienna, where he was teaching and working in research in close collaboration with the industry in the fields of high performance drives, high frequency inverter systems for process technology and uninterruptible power supplies. He has proposed numerous novel converter topologies,

e.g., the VIENNA rectifier and the three-phase ac–ac sparse matrix converter concept. He has published over 200 scientific papers in international journals and conference proceedings and has filed more than 50 patents. He was appointed Professor and Head of the Power Electronics Systems Laboratory, Swiss Federal Institute of Technology (ETH) Zurich, in 2001. The focus of his current research is on novel ac–ac and ac–dc converter topologies with low effects on the mains for telecommunication systems, more-electric-aircraft applications, and distributed power systems utilizing fuel cells. A further main area of research is the realization of ultra-compact intelligent converter modules employing latest power semiconductor technology (SiC) and novel concepts for cooling and EMI filtering.

Dr. Kolar is a member of the IEEE. From 1997 through 2000, he was an Associate Editor of the IEEE TRANSACTIONS ON INDUSTRIAL ELECTRONICS and since 2001 has been an Associate Editor of the IEEE TRANSACTIONS ON POWER ELECTRONICS. He is a member of Technical Program Committees of numerous international conferences in the field (e.g., Director of the Power Quality branch of the International Conference on Power Conversion and Intelligent Motion).